 MCB, vol.2, no.4, pp.217-233, 2005

Systolic Modeling of the Left Ventricle as a Mechatronic System: Determination of Myocardial Fiber's Sarcomere Contractile Characteristics and New Performance Indices

Dhanjoo N. Ghista [1,2], Liang Zhong [2], Leok P.Chua[2], Eddie Y-K Ng[2], Soo T.Lim [3], Ru S. Tan[3], and Terrance S-J Chua[3]

Abstract: **Background**: In this paper, the left ventricle (LV) is modeled as a cylinder with myocardial fibers located helically within its wall. A fiber is modeled into myocardial structural units (MSUs); the core entity of each MSU is the sarcomeric contractile element. The relationship between the sarcomere unit's contractile force and shortening velocity is expressed in terms of the LV model's wall stress and deformation, and hence in terms of the monitored LV pressure and volume. Then, the LV systolic performance is investigated in terms of a mechatronic (excitation-contraction) model of the sarcomere unit located within the LV cylindrical model wall. **Methods**: The governing equation of dynamics of the LV myocardial structural unit (MSU) is developed, involving the parameters of the series-elastic element (SE), the viscous element (VE) and the contractile element (CE). We then relate the MSU's force and displacement variables (in terms of SE, VE and CE parameters) to the LV pressure and volume, using the patient's catheterization-ventriculogram data. We thereby evaluate the MSU elements' parameters. **Results**: We then determine the sarcomere (CE) 'force vs. shortening-velocity' characteristics as well as the power generated by the sarcomere (or CE) element. These are deemed to be important LV functional indices. When our computed sarcomeric peak-power is compared against the traditional LV contractility indices (by linear regression), a high degree of correlation is obtained. **Conclusions**: We have provided herein, a LV systolic-phase (cylindrical geometry) model whose wall contains the myocardial fibers having sarcomere units. We have expressed the LV myocardial sarcomere's CE (force vs. shortening-velocity) characteristics in terms of the LV pressure-volume data. These CE properties express the intrinsic performance capacity of the LV. Hence, indices containing these properties are deemed to reflect LV performance. In this regard, our new LV contractility index correlates very well with the traditional LV contractility index dP/dt_{max}.

keyword: Excitation-contraction, Contractile element, Power, Contractility, Left ventricle.

1 Background

In physiology, several systems are mechatronic in their functional operation, such as the skeletal muscle (SM) excitation-contraction unit (Buckwalter, Einhorn and Simon, 2000), the myocardial sarcomere (Guyton, 1991), the gastro-intestinal (GI) motility system (Hoilet, 1977), and the uterus (UT) contractile apparatus (Bulletti, 2001). The innervated skeletal muscle operates as a coupled excitation-contraction system, whereby the nerve electrically simulates and depolarizes the muscle, which responds to the stimulation by contracting. A contracted muscle develops internal force and shortens if its internal force is greater than the force acting on it. For example, when we want to lift a heavy load (W), we contract our biceps muscle. In this process, the muscle's sarcomere contractile element (CE) develops force (F_{CE}), which is transmitted to the muscle's elastic-element (EE) in series with it and hence to the load. When the developed force F_{CE} exceeds W, the biceps muscle shortens, causing the arm to flex at the elbow and lift the load W (Tan, Zhong, Fuss and Ghista, 2004).

We can extend this simple mechanism to the heart myocardium. Herein, the bioelectrical depolarization wave is generated from the pacemaker cells and spreads over the heart muscle, thereby stepwise depolarizing the heart muscle (or the myocardium) (Guyton, 1991). So, as the

[1] Bioengineering Division, School of Chemistry & Biomedical Engineering, College of Engineering, Nanyang Technological University, Singapore, 639798

[2] School of Mechanical Aerospace Engineering, Nanyang Technological University, Singapore, 639798

[3] Department of Cardiology, National Heart Center, SingHealth, Mistri Wing, 3rd Hospital, Avenue, Singapore, 168572

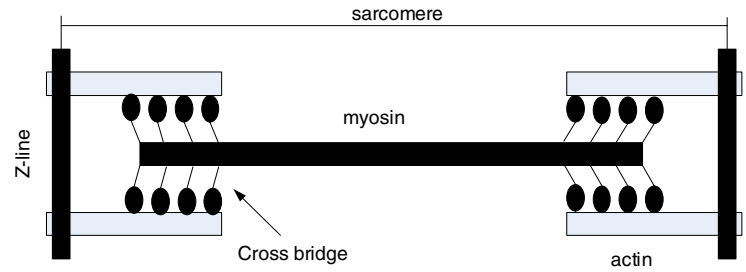

(a)

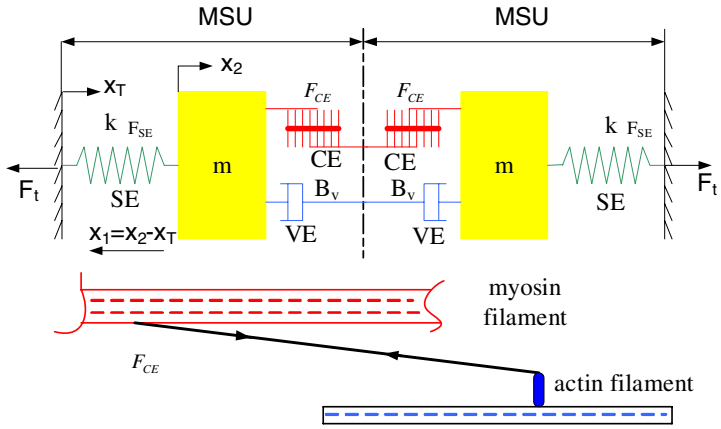

(b)

Figure 1 : (a) The actin and myosin filaments constituting the contractile components of the myocardial fibril; (b) Myocardial fibril model composed of two symmetrical myocardial structural units (MSUs), which are mirror images of each other. Each MSU is composed of (i) an effective mass (m) that is accelerated; (ii) connective-tissue series element having parameter k (elastic modulus of the series element) and the force F_{SE}; (iii) the parallel viscous element of the sarcolemma having viscous damping parameter B_v and force F_{VE}; (iv) the contractile element (CE), which generates contractile force F_{CE} between the myosin (thick) and actin (thin) filaments. When the contractile element shortens (by amount x_2), the series element lengthens (i.e., x_1 increases). During ejection the MSU x_T decreases, and during filling the MSU x_T increases.

bioelectrical wave spreads and propagates through the heart myocardial wall, it causes an analogous myocardial sarcomeric (CE) contractile force wave to propagate through the myocardium. The resulting induced radial stress acting on the inner surface of the heart left ventricular (LV) chamber equilibrates the pressure of the blood in the LV, thereby raising the LV pressure. When the LV chamber pressure exceeds the pressure of blood in the aorta, then the aortic valve opens and the blood is ejected into the aorta and then pumped to the various organs.

2 Purpose, Scope and Assumptions

We note that in all of bio-electro-mechanical physiological systems, the key phenomenon is the excitation-contraction coupling mechanism of the myocardial sarcomere. In this paper, we present a model of myocardial structural unit (MSU), composed of the sarcomere, sarcoplasmic reticulum and the connective tissue. We first analyze the MSU's dynamics in terms of the CE shortening velocity response to contractile force. We then link the MSU's sarcomere contractile force and shortening velocity to the LV monitored pressure and volume data, and derive therefrom indices for left ventricle (LV)

contractility and power.

In order to express the LV myocardial fiber's contractile force and shortening velocity in terms of the monitored pressure and volume, we assume that the cylindrical helically model wall contains N number of myocardial fibers with one set of N/2 fibers wound clockwise and another set counter-clockwise at pitch angle α.

Now, it is not possible for us to determine the invivo value of α across the wall, nor its variation during the cardiac cycle. Hence, herein, we determine the intrinsic equivalent value of α, based on the concept that the force induced in the LV wall's myocardial fibers equilibrates the LV internal pressure. Contraction of the LV is deemed to occur by contraction of one set helically wound α-angled myocardial fibers. When these α-angled helically-wound myocardial fibers contract, they also impart a twist (θ) to the LV which can be monitored by MRI-tagging.

While in this paper, we have not got around to monitoring the twist angle θ for the same patient, yet the order of magnitude of the calculated value of θ based on the contractile force generated in the α-angled myocardial fiber corresponds to the monitored value. This provides credibility to determination of the value of the pitch angle α.

3 Methods

3.1 LV myocardial model

In Figure 1-a, the sarcomere unit of MSU consists of overlapping myosin and actin filaments. The myosin filament is symmetrical about its midpoint, and contains two sets of regular arrays of myosin heads. Muscle contraction is driven by the motor protein II, which binds transiently to an actin filament, generates a unitary filament displacement or "working stroke", then detaches and repeats the cycle (Reconditi, Linari, Lucii, Stewart and Sun, 2004). Sarcomere shortening is generated by the relative sliding of the two filaments, driven by the working stroke of the myosin head.

In Figure 1-b, we define the myocardial fibril model, composed of two myocardial structural units (MSUs) in series. Based on the Hill three-element model (Hill, 1938) and Huxley cross bridge theory (Huxley and Niedergerke, 1954; Huxley, 1974), the sarcomere actin-myosin filaments can be represented by the contractile element of a 3-element MSU model, the connective tissue can be represented by the series-elastic element, while the sarcolemma can be represented by a parallel viscous element, as illustrated in Figure 1-b.

Hence, the biomechanical model of the myocardial structural unit (MSU) consists of the MSU mass, a series-elastic element (SE), a parallel-viscous element (VE) and a contractile-element (CE) (Zhong, Ghista and Ng, 2004). The sarcomere represents the fundamental functional structure of contraction of the MSU. It makes the muscle fiber contract, and generates stress within the wall.

In Figure 1-b, m denotes the myocardial structural unit (MSU) mass; B_v is the viscosity parameter; k is the connective tissue elasticity parameter; x_T is the displacement of the MSU relative to the center line; x_2 is the displacement of the MSU mass due to contraction and resulting shortening of its CE; x_1 is the displacement of SE ($=x_2 - x_T$); F_{CE} denotes the force generated by the CE; F_{VE} denotes the force in the VE; F_t denotes the resulting total MSU force which is related to the chamber pressure of LV.

3.2 LV Cylindrical Model (incorporating the myocardial fibers within its wall)

In this study, the left ventricle (LV) is represented as a thick-walled cylindrical shell. Transverse isotropy is assumed with respect to the axis of the cylinder (Shoucri, 1990, 1998, 2000). In Figure 2, we depict the LV model cylinder, whose wall is composed of N myocardial fibre units (as shown in Figure 2), oriented as helixes of pitch angle α. Half of these (i.e., N/2) fibres are wrapped in a clockwise fashion, and $N/2$ fibers in counter-clockwise fashion. The biomechanical model ultra-structure of each fiber is the MSU, as depicted in Figure 1.

For our LV cylindrical model, we assume that each myocardial model fiber is helically wrapped within the LV cylindrical model wall (as illustrated in figure 2), and composed of two in-series MSUs, as illustrated in Figure 1. In actuality, there will be many myocardial structural units (MSUs) along any one myocardial fiber from bottom to top. However, herein, for convenience of analysis, we adopt each myocardial fiber to be composed of two MSUs in series.

Now although there are a number of myocardial fibers across the LV wall thickness, it is assumed that, within the wall of our LV model, one set (N/2 number) of fibers are oriented in a clockwise fashion, while another equal

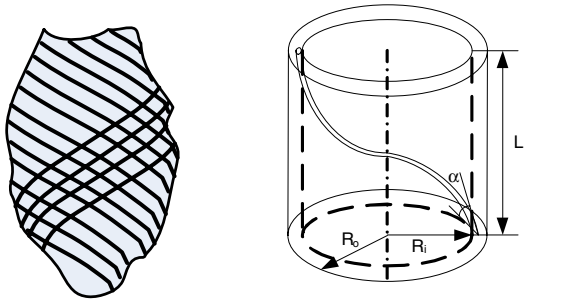

(a) (b)

Figure 2 : (a) Schematic of LV myocardial structure, (b) LV cylindrical model, depicting a typical myocardial fiber arranged as a helix within the LV model wall; L, R_i & R_o are the length, inner and outer radii of the LV cylindrical model.

number (N/2) of fibers are oriented counter clockwise. Hence across the LV wall thickness, we have two fibers, or the LV wall thickness equals two fibers thickness.

The geometric parameters of the LV cylindrical model are defined in Figure 2. The volumes of myocardial wall (MV) and of the LV are given as:

$$MV = \pi(R_o^2 - R_i^2)L = \pi(2R_i + h)hL \quad (1)$$

$$V = \pi R_i^2 L \quad (2)$$

where (i) R_i and R_o are inside and outside radii of the cylindrical model, and (ii) L and h are length and wall-thickness of the model. Herein, the LV volume (V), wall thickness (h) and myocardial volume (MV) are obtained by cineventriculography. Using equations (1 & 2), we can calculate the instantaneous radii $R_i(t)$and length $L(t)$ (or any time instant t) in terms of the measured MV, V and h, as

$$R_i = \frac{2Vh/MV + \sqrt{(2Vh/MV)^2 + 4Vh^2/MV}}{2},$$
$$L = V/\pi R_i^2 \quad (3)$$

Then $R_o = R_i + h$ and $R_m = (R_o + R_i)/2$.

3.3 Determination of (a) fiber density length and force (b) equivalent value of the angle (α) for the LV model, MSU force (F_t), and (c) torque (produced on the LV) due to fiber activation

Now, it is known that the LV twists during systole and unwinds thereafter. This twist is due to the contraction of the myocardial fibers. It is accepted that the fiber angle will vary across the wall thickness and also with time during a cycle. Herein, our LV model, we have adopted that there are two adjacent sets of fibers within the wall thickness, one set oriented clockwise and another set oriented counter clockwise. Each myocardial fiber is assumed to be oriented helically within the LV myocardial wall, at a pitch angle α (as illustrated in Figure 2), with $N/2$ fibers are oriented helically clockwise at pitch angle α, and the other $N/2$ fibers are oriented anticlockwise at the same pitch angle, analogous to that adopted by Pietrabissa et al (1988). We will now determine this fiber angle for our LV model.

A) Fiber density, length and force:

During filling, the fibers will extend as the LV cylindrical model fills with blood. During systole, the fibers will contract and shorten, and twist the LV cylindrical model. Thus the LV will twist and unwind during a cardiac cycle.

In this cylindrical model, there are N myocardial fibres within the LV wall (as shown in figure). Hence:

$$N/2 = \frac{A_{cylinder}}{2A_{msu}} \quad (4)$$

wherein $A_{cylinder}$ (the cross-section area of cylindrical model myocardium) $=\pi(R_o^2 - R_i^2)$ and A_{msu} (the cross-section area of MSU) approximately equals $7.85 \times 10^{-5} cm^2$ (Paladino and Noordergraf, 1988). Although $A_{cylinder}$ varies during a cycle, the number of fibers is deemed to remain constant. Hence we determine the value of N, at say the start of isovolumic contraction, from equation (4).

The activation of these fibers develops active force (F_{CE}) in the sarcomere unit of MSU, which in turn generates wall stress and thereby raises the intra-ventricular pressure. When the pressure exceeds the pressure in the aorta, then the aortic valve opens, the LV shortens (and its wall thickens) to pump an appropriate stroke volume.

The instantaneous length of each myocardial fiber (or myofiber) is given by:

$$l_t = L_t / \sin\alpha_t \quad (5)$$

For instantaneous pressure P(t), the force in a myofiber is given by (with reference to Figure 3)

$$F_t = \pi R_i^2 P_t / (N/2) \sin\alpha_t \quad (6)$$

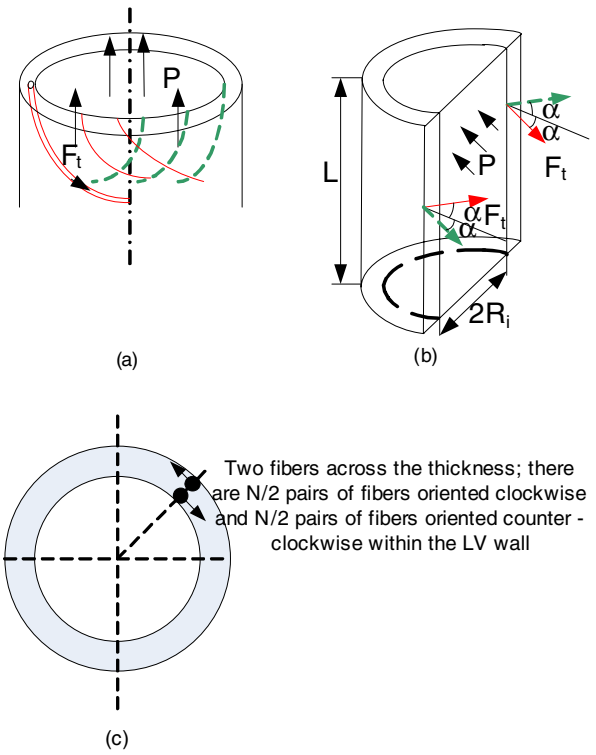

Figure 3 : (a) Equilibrium of fiber force and LV pressure on the top circular plane of the LV cylindrical model, b) Equilibrium of fiber force and LV pressure in the circumferential direction, c) Location of two sets of fibers across the LV wall thickness.

where R_i denotes the instantaneous value of the inner radius of the model obtained from equations (1 & 2)

Therefore, because we have 2 MSUs in series along each myofiber, the axial displacement x_T of a MSU (shown in Figure 1) can be related to the change of length (Δl_t) of a MSU, and hence to the change in length (ΔL_t) of the LV cylinder model as:

$$x_T = \Delta l_t/2 = \Delta L_t/(2\sin\alpha_t) \tag{7}$$

where $\Delta L = L_{t+1} - L_t$, L_{t+1} and L_t refer to successive time instants, and L_t is given by equation (3).

B) Determining the fiber pitch angle α:

We refer to the paper of Pietrabissa et al (1988), wherein the authors demonstrate that the fiber angle for a cylindrical model can be shown to be independent of the LV instantaneous dimensions, and hence can be assumed to be constant throughout the cycle. We now determine this fiber angle α.

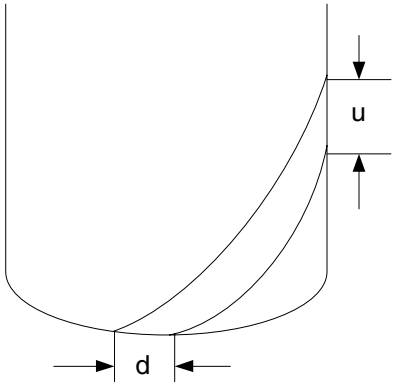

Figure 4 : calculation of u and d.

At any instant, it is assumed that the depolarization wave is travelling along one set of myocardial fibers, i.e. either $N/2$ clockwise or $N/2$ anticlockwise oriented fibers. The contraction of one set (N/2) of these fibers hence results in a clockwise or anti-clockwise twist of the LV. The distance (d) along a circumference between two adjacent fibers arranged in the same direction (i.e., clockwise or counter-clockwise) is given by (with reference to Figure 4):

$$d = 2\pi R_i/(N/2) = 4\pi R_i/N \tag{8}$$

The axial pitch (u) between the fibres arranged in the same direction intersected by a cylinder generatrix is given by:

$$u = L/(n/2) = 2L/n \tag{9}$$

wherein $n/2$ is the number of fibers arranged in the same direction intersected by a cylinder generatrix

From equations (8) and (9)

$$\frac{u}{d} = \tan\alpha = \frac{LN}{2\pi R_i n} \tag{10}$$

In Figure 3(a), the equilibrium of axial forces in one set of fibers arranged in the same direction, acting on the bottom or top circular plane surface of the LV model cylinder, requires that the sum of the vertical components of the fiber forces equilibrates the force due to LV pressure acting on the LV top (or bottom) surface. Hence, as indicated before (by equation 6)

$$\pi R_i^2 P = (N/2)(F_t \sin\alpha) \tag{11}$$

where P is the LV cavity pressure and F_t is the force within each of the N fibres.

In Figure 3(b), the equilibrium of the cylinder in circumferential direction, under the action of fiber forces arranged in the same direction, requires that:

$$(2LR_i)P = nF\cos\alpha \tag{12}$$

Upon substituting equations (11) and (12) into equation (10), we obtain the equivalent fiber-angle (α) for the LV as follows

$$\tan\alpha = 1/\sqrt{2} \tag{13}$$

which yields α=35.26°

C) Torque impacted to the LV by fiber contraction:

At this point, it is noteworthy that (on the basis of figure 3-a), while the vertical components of the fiber forces equilibrate the pressure in the chamber (as per equation 7), their horizontal components produce a torque (T) in the LV, given by:

$$\begin{aligned} T_t &= (N/2)F_t\cos\alpha_t \\ &= \frac{(N/2)\pi R_i^2 P_t\cos\alpha_t}{N/2\sin\alpha_t} \\ &= \pi R_i^2 P_t ctg\alpha_t \end{aligned} \tag{14}$$

This torque (T_t) will result in a twist of the LV by angle θ_t given by:

$$\theta_t = \frac{T_t L_t}{JG} = \frac{\pi R_i^2 P_t L_t (ctg\alpha_t)}{JG} \tag{15}$$

where L_t is the instantaneous length of the LV cylindrical model, α_t (=α) is given by equation (13), J (the polar moment of inertia)=$\pi(R_o^4 - R_i^4)/2$, and G (the shear modulus of the LV myocardium)≅ 100 Gpa (Ionescu et al, 2005). This means that for a 60 mmHg pressure rise during isovolumic contraction, a LV model (having R_i=2cm, R_o=3cm and L=14cm) will twist by an amount of 10°, and by 20° up to the instant when the LV pressure becomes maximum. After that, the LV will rewind. These calculated twist angles correspond to the monitored values (Xia et al, 2005), thereby linking some credibility to our model.

Equation (15) indicates that if we can measure the twist angle θ (of the apex of the LV with respect to its base) by MRI-tagging, then we can also determine the value of the fiber angle α corresponding to the monitored LV pressure. Hence, we do not need to adopt α to stay constant during a cardiac cycle. Hence, although in this paper, we have taken α to be constant during a cardiac cycle, in our subsequent works we can compute the instantaneous value of α from equation (15). However, at this stage, we are in a position to only obtain data on LV pressure and volume and not on the twist angle. We have started to determine this twist angle θ, and found that it varies by about 10^o during systole, which corresponds to the value obtained from equation (15).

It can be conceptually noted that for certain R_i and L_i, the in-vivo value of θ during a cardiac cycle influences the value of P_t generated. However, for the sake of demonstrating the prime purpose of this model-analysis (namely to demonstrate how we can relate the sarcomere contractile force and shortening velocity to LV pressure & volume data and compute these sarcomere parameters), we adopt the angle α to remain constant throughout the cycle (even though we concede that this is not true in practice).

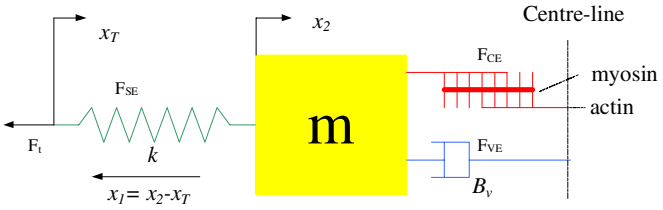

Figure 5 : Dynamic model of MSU having effective mass m; k is the elastic modulus of series element; B_v is the viscous-damping parameter of parallel viscous element; F_t denotes the total generated force caused by the contractile stress F_{CE}; F_{SE} is the force in the series element ($= k(x_1 + x_{1ed})$), where x_{1ed} is the deformation of the SE at end-diastole; F_{VE} is the force in the viscous element ($= B_v\dot{x}_2$); x_1 then represents the added deformation of the SE during systole (over and above its deformation during the filling phase) due to the development of F_{CE}. As shown in Figure 5, each myocardial fiber from bottom to top edge of the LV myocardial model is composed of two MSUs. The governing differential equation for this model is given by equations (16 & 17).

3.4 Dynamics of a myocardial structural unit

A) Governing equation of MSU dynamics and its solution

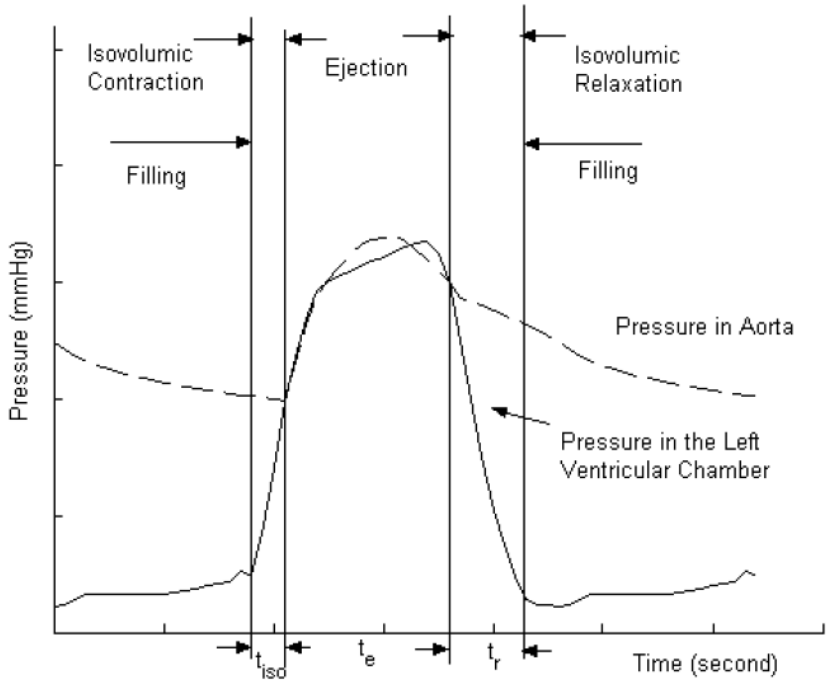

Figure 6 : Schematic of LV pressure and aortic pressure variation during a cardiac cycle.

From Figure 5, the governing differential equation for a MSU dynamics, due to the generated contractile force (F_{CE}), can be expressed as:

$$m\ddot{x}_2 + B_v\dot{x}_2 - F_{CE} + kx_1 = 0 \tag{16}$$

or,

$$m\ddot{x}_1 + B_v\dot{x}_1 + kx_1 = F_{CE} - B_v\dot{x}_T - m\ddot{x}_T \tag{17}$$

where,

F_{CE} is the applied force exerted by the contractile-element of MSU;

m is the muscle mass per unit cross-section area = $\pi(R_o^2 - R_i^2)L\rho/2N$, ρ is muscle density;

B_v is the viscous damping parameter of the parallel viscous element (VE);

k is the elastic stiffness (or modulus) of the series-elastic element (SE);

x_T is the shortening displacement of the myocardial-fiber unit relative to its centre-line;

x_1 is the stretch of the SE element, $= x_2 - x_T$;

x_2 is the displacement of muscle mass m (relative to centre-line) due to CE contraction, $= x_T + x_1$;

$F_{VE} = B_v\dot{x}_2$, and $F_{SE} = k(x_1 + x_{1ed})$;

x_{1ed} is x_1 at end-diastole ($= F_{ted}/k$);

F_{ted} is the fibre force at end-diastole, obtainable from equation (12) corresponding to R_i and P at end-diastole.

Because the terms $m\ddot{x}_1$ and $m\ddot{x}_T$ can be neglected due to their small values compared to other terms (for instance, $m\ddot{x}_1$ and $m\ddot{x}_T$ are of the order of 10^{0-1} while the other terms are of the order of 10^{3-4}) (Zhong et al, 2004), equation (17) can thus be rewritten as:

$$B_v\dot{x}_1 + kx_1 = F_{CE} - B_v\dot{x}_T \tag{18}$$

Now, let us consider myocardial contraction during the systolic phase. The systolic contraction can be considered to comprise of two temporal phases. Phase I, denoted by t_{iso} (and measured in seconds), corresponds to isovolumic contraction; it comprises the interval from the closing of the mitral valve until the opening of the aortic valve. Phase II, denoted by t_e, corresponds to the ejection phase, as shown in Figure 6.

Now let us discuss the right-hand terms of equation (18). As the MSU (and LV) depolarizes, excitation-contraction coupling leads to sarcomere contraction and the development of ventricular wall stress, along with a rapid increase in intraventricular pressure as shown in Figure 6. During this phase of systolic contraction, let us express the generated **MSU-CE force** (F_{CE}) function

(analogous to the LV pressure wave shape) as:

$$F_{CE} = F_{CE0}\sin(\omega_{ce}t)e^{-z_{ce}t} \tag{19}$$

where $\omega_{ce} = \pi/t_s$; t_s is the contraction duration, to be determined; F_{CE0} and z_{ce} are the additional parameters, to be determined; t=0 corresponds to the start of isovolumic contraction phase. It should be noted that this expression for F_{CE} is similar to that for the active elastance of our earlier paper (Zhong et al, 2005).

Let us now discuss the x_T terms on the right hand side of equation (18). During the filling phase, the MSU will stretch passively due to LV enlargement. Concerning the x_T term, during the filling phase, x_T will be negative and its absolute value will increase due to passive stretching of the myocardial fibers caused by LV volume increase. During this phase, within reference to Figure 5, the SE element will stretch while x_2=0, and hence x_1=-x_T. At the end of filling phase, we denote x_1 by x_{1ed}. Further increase in x_1 now occurs during isovolumic contraction due to development of F_{CE} and the generation of CE shortening (x_2). However, in this phase x_T=0, and hence x_1^{iso} is only due to x_2 caused by F_{CE}.

During the ejection phase, x_T is positive and is caused by LV ejection and volume decrease. At the same time, x_2 is being generated by CE contraction and F_{CE} development. Somewhere during the ejection phase, x_2 will reach its maximum value and thereafter decrease. Now during the isovolumic relaxation phase, x_2 keeps decreasing, while x_T does not change from its end-ejection value.

When the filling phase starts, x_T again becomes negative and $|x_T|$ starts increasing as the LV volume increases. Meanwhile x_2 keeps decreasing and reaches a zero value, a short while after the start of filling phase at t=t_o. This time period t_o is designated as the LV suction phase caused by deceasing F_{CE}, before the left atrium starts to contract and pump blood with the LV. Herein, we will demonstrate this suction effect in terms of t_0.

Phase I: Solving equation (18) for isovolumic contraction phase (during $0 < t < t^{iso}$):

Since both the mitral and aortic valves are closed, the volume of blood in the ventricle is constant. Yet the pressure inside LV is increasing due to the sarcomere contraction, i.e., due to F_{CE} generation. Hence putting $x_T = \dot{x}_T = \ddot{x}_T = 0$, and employing F_{CE} from equation (19), we can rewrite equation (18) as:

$$B_v\dot{x}_1 + kx_1 = F_{CE0}\sin(\omega_{ce}t)e^{-z_{ce}t} \tag{20}$$

The solution of equation (20) is given by $x_1(=x_1^{iso})$, as follows:

$$\begin{aligned} x_1(t) &= x_1^{iso}(t) \\ &= C_1e^{-k/B_vt} + [a\sin(\omega_{ce}t) + b\cos(\omega_{ce}t)]e^{-z_{ce}t} \end{aligned} \tag{21}$$

where $a = \frac{F_{CE0}(k - z_{ce}B_v)}{(k - z_{ce}B_v)^2 + (B_v\omega_{ce})^2}$, $b = -\frac{F_{CE0}B_v\omega_{ce}}{(k - z_{ce}B_v)^2 + (B_v\omega_{ce})^2}$.

For this phase of contraction, the initial condition that we will impose is:

$$x_1^{iso}(0) = C_1 + b = 0 \tag{22}$$

from which

$$C_1 = -b \tag{23}$$

Hence, x_1 ($=x_1^{iso}$) during the isovolumic contraction phase is given by

$$\begin{aligned} x_1(t) &= x_1^{iso}(t) \\ &= (-b)e^{-k/B_vt} + [a\sin(\omega_{ce}t) + b\cos(\omega_{ce}t)]\,e^{-z_{ce}t} \end{aligned} \tag{24}$$

Phase II: Expression for x_T and solving equation (18) for ejection phase to determine parameters x_{T0} and z_e

For mathematical convenience, we make a shift in the time variable and redefine it as $t_a = t - t_{iso}$, such that

$$0 \le t_a \le t_e \tag{25}$$

where t_e is the ejection phase duration.

In this phase,$x_T$is no longer zero, and hence we need to relate it to the LV dimensional change, as per equation (13), as:

$$x_T = \Delta l_t/2 = (L_{(t+1)} - L_t)/2\sin\alpha \tag{26}$$

wherein L_t and L_{t+1} refer to successive time instants t_i and t_{i+1}, and L_i (or L) is given by equation (3) in terms of V, MV and h.

We now adopt a functional expression for $\dot{x}_T$ function (to correspond to the shape of the LV flow-rate $\dot{V}$), as per our earlier formulation for $\dot{V}$ to be (Zhong et al, 2004), as follows:

$$\dot{x}_T = x_{T0}\sin(\omega_e t_a)e^{-z_e t_a} \tag{27}$$

where $\omega_e = \pi/t_e$, t_e is the duration of ejection as shown in Figure 6; x_{T0} and z_e are the (to-be-determined) parameters, and $t_a = 0$ corresponds to the start-of-ejection phase.

By integrating equation (27), and employing the initial condition of $x_T(t_a = 0) = 0$, we get

$$x_T = -\frac{x_{T0}}{z_e^2+\omega_e^2}\left[z_e \sin(\omega_e t_a) + \omega_e \cos(\omega_e t_a)\right] e^{-z_e t_a} + \frac{x_{T0}\omega_e}{z_e^2+\omega_e^2} = \Delta l_t/2 = (L_{i+1} - L_i)/2\sin\alpha \quad (28)$$

Now, based on equation (29), x_T can be evaluated in terms of Δl_t and hence in terms of monitored $h(t)$, $V(t)$ and *MV*. *Hence, the parameters x_{T0} and z_e (of $\dot{x}_T$ in equation 28) can be obtained by matching the x_T expression of equation (29) with the clinically obtained MSU length-change $\Delta l_t/2$, as indicated by equation (29). This then enables us to also determine the expression $\dot{x}_T$ (equation 28) in terms of its now evaluated parameters x_{T0} and z_e.*

Then, by substituting equations (20 & 28) into the governing equation (18), we have:

$$B_v\dot{x}_1 + kx_1 = F_{CE0}\sin(\omega_{ce}(t_a + t_{iso}))e^{-z_{ce}(t_a+t_{iso})} - B_v x_{T0}\sin(\omega_e t_a)e^{-z_e t_a} \quad (29)$$

where t_a is the time variable. **The solution of equation (29) is given by** $x_1(= x_1^e)$, as follows:

$$x_1(t_a) = x_1^e(t_a) = C_2 e^{-k/B_v t_a} + \left[a\sin(\omega_{ce}(t_a+t_{iso})) + b\cos(\omega_{ce}(t+t_{iso}))\right] e^{-z_{ce}(t_a+t_{iso})} + \left[c\sin(\omega_e t_a) + d\cos(\omega_e t_a)\right] e^{-z_e t_a} \quad (30)$$

where,

$$a = \frac{F_{CE0}(k - z_{ce}B_v)}{(k - z_{ce}B_v)^2 + (B_v\omega_{ce})^2},$$

$$b = -\frac{F_{CE0}B_v\omega_{ce}}{(k - z_{ce}B_v)^2 + (B_v\omega_{ce})^2},$$

$$c = -\frac{B_v x_{T0}(k - B_v z_e)}{(k - B_v z_e)^2 + (B_v\omega_e)^2},$$

$$d = \frac{B_v^2 x_{T0}\omega_e}{(k - B_v z_e)^2 + (B_v\omega_e)^2}$$

In equation (31), the unknown parameters are k, $B_v, F_{CE0}, \omega_{ce}$ and z_{ce}.

Now $x_1(t)$between phases I and II is continuous, i.e., $x_1^e(t_a = 0) = x_1^{iso}(t = t_{iso})$. This determines the initial condition for phase II. Hence, from equations (25 & 31), we get:

$$\begin{aligned} x_1^e(0) &= C_2 + [a\sin(\omega_{ce}t_{iso}) + b\cos(\omega_{ce}t_{iso})]e^{-z_{ce}t_{iso}} + d \\ &= x_1^{iso}(t = t_{iso}) \\ &= -be^{-k/B_v t_{iso}} + [a\sin(\omega_{ce}t_{iso}) + b\cos(\omega_{ce}t_{iso})]e^{-z_{ce}t_{iso}} \end{aligned} \quad (31)$$

Solving equation (32), we get

$$C_2 = -be^{-k/B_v t_{iso}} - d \quad (32)$$

Hence, **the total SE deformation** $x_1(= x_1^e)$during the ejection phase (on top of x_1 at t^{iso} the end of isovolumic contraction, given by equation 25) can be written as:

$$x_1(t_a) = x_1^e(t_a) = (-be^{-k/B_v t_{iso}} - d)e^{-k/B_v t_a} + \left[a\sin(\omega_{ce}(t_a+t_{iso})) + b\cos(\omega_{ce}(t_a+t_{iso}))\right] e^{-z_{ce}(t_a+t_{iso})} + \left[c\sin(\omega_e t_a) + d\cos(\omega_e t_a)\right] e^{-z_e t_a} \quad (33)$$

B) Obtaining solutions for the model parameters (k, B_v, F_{CE0}, ω_{ce}, z_{ce})

Having determined the parameters x_{T0} and z_e from equation (29), by matching x_T with Δl, we will now determine the remaining parameters k, B_v,F_{CE0}, ω_{ce} and z_{ce} (in equation 21) On the basis of Figures 2 & 3 and equations (12 & 18), we put down

$$F_{SE} = F_t = k(totalSEdeformation) = k(x_{1ed} + x_1^e) = F_{ted} + kx_1^e \quad (34)$$

where (i)x_1^e during the ejection phase is given by equation (34), (ii)x_{1ed} (x_1 at end-diastole) is given by equation (18), and (iii) F_t and F_{ted} are obtained in terms of LV pressure, model geometry, fiber angle (α) and N from equation (12). Hence,

$$k \cdot x_1^e = F_t - F_{ted} = 2\pi R_i^2(P - P_{ed})/(N\sin\alpha) \quad (35)$$

wherein the x_1^e expression is given by equation (34). We now match the expression for kx_1^e (of equation 34) with the evaluated value of the right-hand side term of equation 36 in terms of clinical-derived data (of LV pressure, R_i and N) of the subject. By carrying out parameter-identification, we can determine the corresponding parameters $k$as well as$B_v, F_{CE0}, \omega_{ce}$ and z_{ce}(in equation 34). Once we know the values of these parameters, we can determine the values of the x_1^e during the ejection phase.

3.5 *Sarcomere force, shortening velocity, power and contractility*

A) Determining sarcomere contractile F_{CE} and x_2, and their physiological implications

Having evaluated the parameters (k, B_v, F_{CE0}, ω_{ce}, z_{ce}) in section 2.4(B), we can determine the CE contractile force F_{CE} from equation (19), as well as x_1 during isovolumic contraction (from equation 25) and during ejection (from equation 34). The shortening displacement of CE, x_2 (=$x_1 + x_T$) can also be computed by employing (i) x_1 from equation (34) in terms of its evaluated parameters k, B_v,F_{CE0}, ω_{ce} and z_{ce}, and (ii) x_T from equation (29) in terms of its evaluated parameters x_{T0} and z_e. Now, for a total variation of x_2 during a cardiac cycle, we adopt the x_2 expression as:

$$x_2 = x_{2o}\sin(\omega_{ce}t)e^{-z_2 t} = x_1 + x_T \tag{36}$$

where x_1 has been computed based on equation (34), x_T is given by equation (29), and t=0 corresponds to the start of isovolumic contraction phase. Hence, in equation (31), we can now evaluate the additional parameters x_{2o} and z_2 by parameter-identification.

Myocardial fiber shortening x_2 is an important cardiac performance variable. It would be interesting to determine the instant (t_o) within the filling-phase, when x_2 becomes zero. From a cardiac physiological viewpoint, during this time-interval (from the start of filling up to instant t_o), the left ventricular pressure value will be below the value at the start of filling phase. This time period from the start of filling phase up to t_o is denoted as the LV suction phase [19].

Hitherto, it has been difficult to provide an explanation for this **suction phase**. However, it can be explained in terms of the continuing activation of FCE into the filling phase from equations (36, 20 & 37), as follows:

$$\begin{aligned} 2\pi R_i^2(P_t - P_{ed})/N\sin\alpha &= F_t - F_{ted} \\ &= F_{SE} - F_{ted} = F_{CE} + F_{VE} - F_{ted} \\ &= F_{CE0}\sin(\omega_{ce}t)e^{-z_{ce}t} + B_v[x_{20}\sin(\omega_{ce}t)]e^{-z_2 t} - F_{ted} \end{aligned} \tag{37}$$

In equation (37), we have determined the parameters of F_{CE} and F_{VE} from the monitored LV pressure P_t. As per equation (37), it is F_{CE} (due to sarcomere contraction) that intrinsically governs the generation of this pressure P_t. Hence it is the continuing activation of CE into the filling phase that causes LV suction and temporal dip in LV pressure before the left atrium contracts and pumps blood into the LV. Later on, we will demonstrate the suction effect in terms of t_0.

B) Power Generated by the Sarcomere Contractile-element

Now, because we have incorporated 2 MSU(s) in each myocardial fibre (as illustrated in Figure 2), we now define the LV myocardial instantaneous power in terms of the MSU CE force causing shortening by amount x_2 and shortening rate of $\dot{x}_2$, as:

$$Power = 2\times(N/2)(F_{CE}\times\dot{x}_2) = N(F_{CE}\times\dot{x}_2) \tag{38}$$

where (i) both F_{CE} and $\dot{x}_2$ are functions of time, (ii)F_{CE} is the contractile force generated by each contractile element, and (iii) $\dot{x}_2$ is the shortening velocity of the CE element. In this equation, N is computed from equation (10);F_{CE} is computed from equation (19), with its parameters (F_{CE0}, $\omega_{ce}$and z_{ce}) obtained from equation (35) by parameter-identification scheme; $x_2 = x_1 + x_T$, with x_1 and x_T computed from equations (34) & (29), respectively. The total Contractile Power-Input (TCPI) is then obtained as:

$$TCPI = N\int F_{CE}d\dot{x}_2 \tag{39}$$

i.e., by the area under the F_{CE} vs. $\dot{x}_2$ curve.

C) Defining a New Contractility Index based on the Contractile Power

Herein, in quantifying the contractile performance of the LV, we define contractility (corresponding to the traditional contractility index of dP/dt_{max}) as the ability of the LV myocardium to produce a contractile force with a high shortening-velocity capability, so as to exert maximum contractile power ($Power_{\max}$). In order to compare $Power_{\max}$ among patients of differing LV size and mass, we now define a new LV contractility index in terms of myocardial sarcomere power (*MSPI*), as:

$$MSPI = Power_{\max}/MV \tag{40}$$

where MV is LV wall-volume, and $Power_{max}$ is the maximal value of power (equation 38). If MV is in cm^3, we can evaluate MSPI in *Watt/litres*.

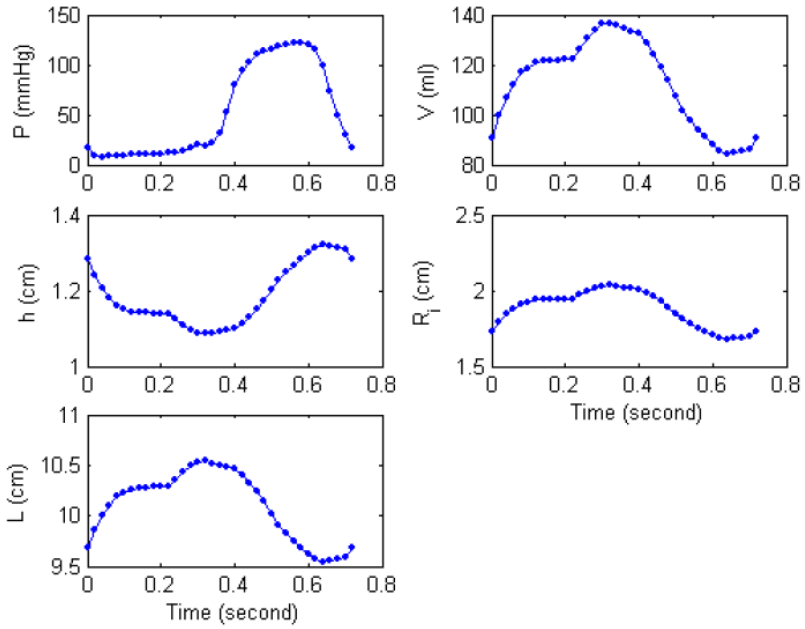

Figure 7 : LV Pressure variation and LV (thick-wall cylinder) model dimensions variations, during a cardiac cycle for subject HEL. MV=185 ml.

Table 1 : Clinical history, measured hemodynamic data from subjects (HEL, DDM and TPS). Where LVP: left ventricle chamber pressure, AOP: aortic pressure, EDV: end-diastolic volume, ESV: end-systolic volume, EF: ejection fraction, MI: myocardial infarct, DVD: double vessel disease, HTN: hypertension, LAD: left artery disease

Subject	HEL	DDM	TPS
Disease	MI, DVD	DVD, HTN	LAD, and Ischemia
LVP (mmHg)	122/18	170/24	147/22
AOP (mmHg)	125/75	169/99	140/71
EDV/ESV (ml)	132.5/84.3	121.7/41.3	112/35.5
EF	0.36	0.66	0.68

4 Clinical Application and Results

The analysis is now applied to the clinically obtained data of the subject's left ventricular (instant-of-instant) dimensions (obtained by cineangiocardiograph) and chamber pressure (obtained by cardiac catheterization). In so doing, for each subject's left ventricular data, we evaluate the model parameters F_{CE} and x_2, the contractile power input (CPI) and the new contractility index MSPI.

Table 1 lists the measured hemodynamic variables for three subjects (subject HEL, DDM, and TPS). Subject HEL serves as a representative of a patient with myocardial infarct. Subject DDM is an example of a patient with double vessel disease (DVD) and hypertension, treated with PTCA. Subject TPS corresponds to a patient with native LAD, ischemia in anterior territory and mitral regurgitation (MR). These three subjects have also been studied by our earlier analysis of passive and active elastance computation [17]. Figure 7 depicts one-sample cineangiocardiographically-derived LV dimensions and the derived cylindrical model dimensions during a cardiac cycle.

4.1 Evaluation of the model parameters

From the clinical data shown in Figure 7, we calculate the LV model x_T, using equation (26). This 'x_T versus time' function during ejection is shown in Figure 8, as illustrated by the round points. We then use the expression of x_T given by equation (29) to fit this clinical derived data of 'x_T versus t', and determine the parameters x_{T0} and z_e, as shown in Figure 8. The model computed x_T matches the x_T $(=(L_{i+1}-L_i)/2\sin\alpha)$ clinical data very

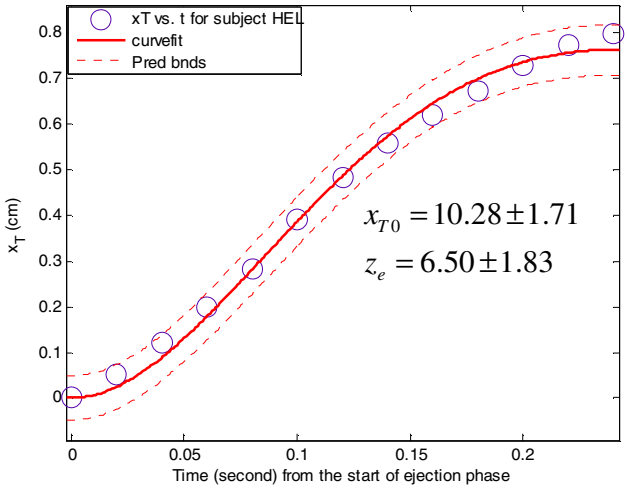

Figure 8 : Computed $x_T(t)$ during the ejection phase (t=0 corresponds to start-of-ejection): From the data shown in Figure 8, we calculate the model x_T during the ejection phase by using equation (11), as shown by the round points in the figure. This data is now fitted with equation (29). The resulting values of the parameters (x_{T0} and z_e) are shown in the figure and also listed in Table 2. Here t=0 corresponds to start-of-ejection.

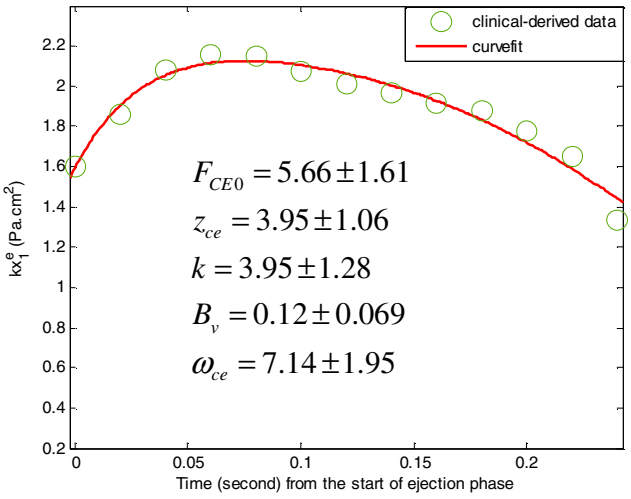

Figure 9 : Computed kx_1^e and its parameters during the ejection phases (t=0 corresponds to start-of-ejection). From the data shown in Figure 7, we calculate the LV model myocardial force F_t and F_{ted} using equation (10). Then we compute$kx_1^e (= (F_t - F_{ted})/N) = 2\pi R_i^2 (P - P_{ed})/N \sin\alpha$, as shown by the round points in this figure, with $N = 2.24 \times 10^5$ from equation (8). This clinical-derived data of $(F_t - F_{ted})/N$ is now fitted with kx_1^e expression (based on equation 34), to obtain the values of kx_1^e parameters (F_{CE0}, z_{ce}, k, B_v, ω_{ce}) listed in the figure as well as in Table 2. Herein, t=0 corresponds to start-of-ejection.

well, with R-square=0.9944 and RMS=0.02 cm. The solid line is the model-computed displacement x_T (equation 29), while the round points constitute the clinical derived x_T.

Now, we use the LV pressure and R_i data in Figure 7, along with calculating N (by equation 10), to obtain the right-hand side of the equation (35), and to **hence evaluate the term** kx_1^e. Since the expression for x_1^e is given by equation (34), we can now employ the parameter-identification scheme to make the kx_1^e expression (equation 34) fit the values of kx_1^e $(=2\pi R_i^2 (P - P_{ed})/N \sin\alpha)$, and compute the other parameters k,$\boldsymbol{B_v}$,F_{CE0}, ω_{ce} and z_{ce}, (as listed in Table 2). In Figure 9, we have shown how the kx_1^e expression (34) matches the computed values of kx_1^e, to evaluate the parameters $k, B_v, \sigma_{CE0}, \omega_{ce}$ and z_{ce}.

4.2 Determination of CE force F_{CE} and shortening x_2 characteristics, with determination of the LV suction effect

Shown in Figure 10 are the computed values of MSU dynamics terms for subject HEL. Figure 10-a provides the measured data of LV pressure in one cardiac cycle. By means of the values of the parameters ($k, B_v, \sigma_{CE0}, \omega_{ce}$ and z_{ce}) in Table 2, we have determined and plotted x_1 vs time, $x_2$vs time, and x_T vs time, in Figure 10-b. The computed CE shortening-velocity ($\dot{x}_2$) and force (F_{CE}) are shown in Figures 10-c & 10-d respectively. Notice that the CE force variation during systole is similar to that of LV active elastance in our earlier paper (Zhong, 2005).

Now we adopted the expression x_2 given by equation (36) in order to project the time-duration (t_0) of sarcomere

Table 2 : Computed values of MSU terms x_T and x_1, and of their parameters related to the subject HEL shown in Figure 7, during ejection phase (N=2.24×10^5).

Variable	Parameters	Values	How obtained	RMS
x_T	x_{T0}(cm)	10.28±1.71	x_T fit using equation (29)	0.02 cm
	z_e (s^{-1})	6.50±1.83		R-square
				0.99
x_1^e	F_{CE0} ($Pa\cdot cm^2$)	5.66±1.61	kx_1^e fit using equation (35)	RMS
				0.028 $Pa\cdot cm^2$
	z_{ce} (s^{-1})	3.95±1.06		R-square
	B_v ($Pa\cdot cm\cdot s$)	0.12±0.069		
	$k(Pa\cdot cm)$	3.95±1.28		0.97
	ω_{ce} (s^{-1})	7.14±1.95		
x_2	x_{20}	0.55±0.01	x_2 fit using equation (36)	0.01
	z_2	-3.03±0.12		0.99

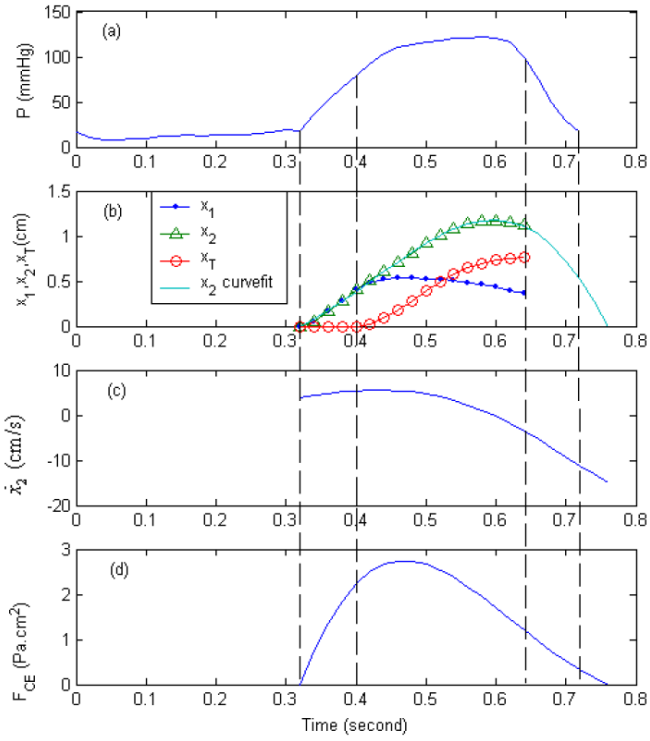

Figure 10 : Computed results of MSU model-dynamics terms x_1, x_2, x_T, $\dot{x}_2$ and F_{CE}, for subject HEL. Diastolic phase: 0-0.32s; isovolumic contraction phase: 0.32-0.4s; ejection phase: 0.4-0.64s; isovolumic relaxation phase: 0.64-0.72s. Here t=0 corresponds to start-of-filling. Note that FCE and x_2 extend into the filling phase; t_0=0.04seconds.

shortening continuing into the filling phase. We can now see, from Figure 10-b, that this duration is 0.04 seconds. This validation and quantification of the LV suction effect is an important added finding of our model analysis.

4.3 Computing total CE contractile power input (TCPI) and contractility index (MSPI)

Next, we also plot the 'force vs. shortening' and the 'force vs. shortening velocity' for the contractile-element (CE) after the initiation of isovolumic contraction phase, as shown in Figures 11 & 12.

Figure 11 is the "CE force vs shortening" characteristic. The CE shortening (x_2) reaches its maximum value late in the ejection phase. The area encircled by force-displacement curve and x-axis represents the CE energy input.

In Figure 12, the CE shortening velocity increases, along with increasing CE force. They both reach their maximum values at about one-third ejection, and thereafter decrease. The area encircled by the curve, multiplied by the number of fibers (N) gives us the TCPI.

From this figure, we can again note that the contractile element stays activation for 0.04 (=0.76-0.72) seconds into the filling phase. This causes LV suction of blood, even prior to the initiation of left atrial contraction

From Figure 12, we calculate total contractile power input (TCPI) to be $5.40W$. The maximum value of instantaneous power, $Power_{\max}$ (equation 38), is computed to be 3.32 W. Using this value, we now calculate the contractility index **MSPI** (equation 40) to be 17.94 W/l.

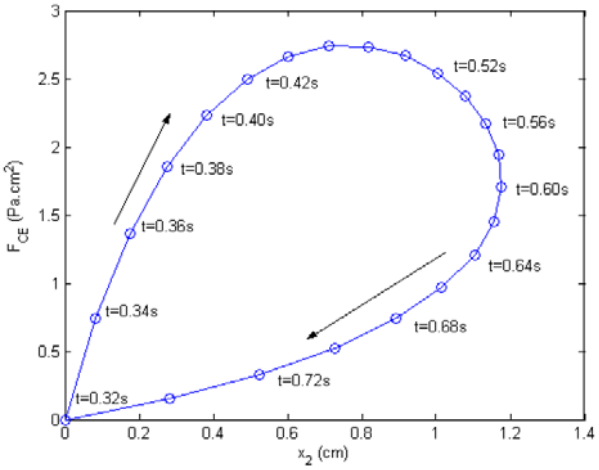

Figure 11 : CE Force (F_{CE}) vs. displacement (x_2) relationship for subject HEL. The arrow direction indicates progression of time, starts from diastolic-filling phase. Here, t=0 corresponds to start-of-filling, the time t=0.32 corresponds to the start of isovolumic-contraction phase. The CE shortening (x_2) becomes zero at t=0.76 second, about 0.04 seconds into the filling phase.

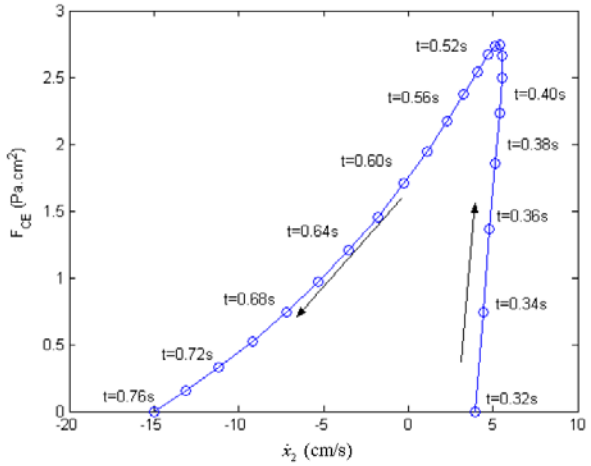

Figure 12 : CE Force (F_{CE}) vs. shortening-velocity ($\dot{x}_2$) relationship for subject HEL. The arrow direction indicates progression of time, starts from diastolic filling phase. Here, t=0 corresponds to start-of-filling, the time t=0.32 corresponds to the start of isovolumic-contraction phase. The next-cyclic filling phase starts at t=0.72second, while F_{CE} becomes zero at t=0.76. In other words, the LV suction effect lasts for about 0.04 second into the filling phase. If we observe the LV pressure variation in Figure 11-a, we can note that the LV pressure in fact decreases after initiation of filling phase and recovers to the level of the start of filling phase after about 0.04 second. To determine the LV Power-Input, we determine the area under this curve and multiply it by N. This gives LV Power-Input=5.40W.

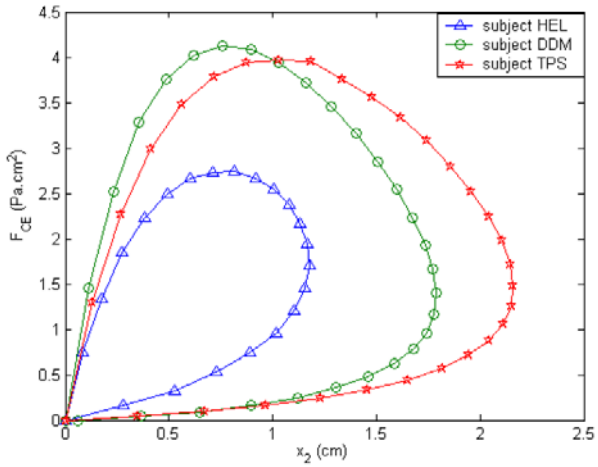

Figure 13 : CE Force (F_{CE})-displacement (x_2) for subjects HEL, DDM and TPS. Of the three subjects, TPS has the biggest area encircled by the F_{CE}vs $x_2$curve; hence, this subject's CE is generating higher energy relative to the other two subjects.

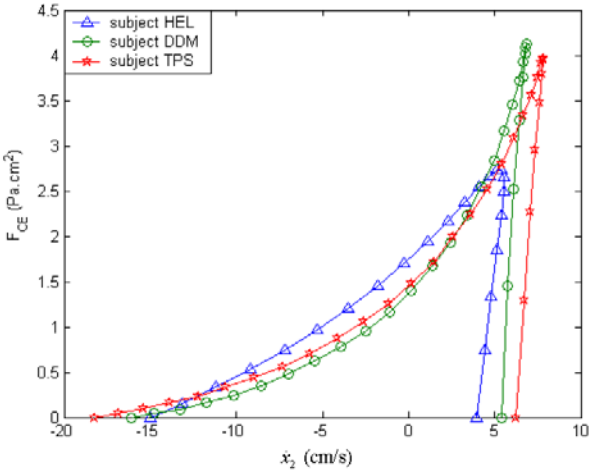

Figure 14 : CE Force (F_{CE})-velocity ($\dot{x}_2$) relationships for subjects HEL, DDM and TPS. Of the three subjects, the subject TPS has the biggest area encircled within the F_{CE} vs $\dot{x}_2$ curve, and hence has the bigger contractile power input.

Table 3 : Table 3: Clinical history, $(dP/dt)_{\max}$, Maximal contractile force,F_{CE}, shortening velocity $\dot{x}_2$ of CE, area under F_{CE} vs. x_2, calculated maximum Power ($Power_{\max}$), TCPI, myocardial volume (MV), left ventricular contractility index (MSPI), from subjects (HEL, DDM, and TPS).

Subject	HEL	DDM	TPS
Disease	MI, DVD	DVD, HTN	LAD, Ischemia
EF	0.36	0.66	0.68
$dP/dt_{\max}$(mmHg/s)	984	1475	1478
MV (ml)	185	138	140
Maximum F_{CE} $(Pa \cdot cm^2)$	2.74	4.12	3.98
Maximal shortening velocity $\dot{x}_2$(cm/s)	5.55	6.84	7.82
TCPI (W)	5.40	5.97	6.33
Power$_{max}$ (W)	3.32	5.18	5.48
MSPI ((W/l)	17.94	37.53	39.14

5 Discussion: comparison of CE performance characteristics for 3 patients, and correction of MSPI with dP/dt$_{max}$

5.1 Computation of CE performance characteristics for other subjects

This analysis is now carried out for two other subjects (DDM and TPS) listed in Table 1, and the results are provided in Table 3. For these subjects, the TCPIs are 5.18W and 5.48 W. Figures 13 and 14 depict the computed CE force vs shortening and CE force vs shortening-velocity characteristics for subjects **HEL** (with MI, DVD), **DDM** (DVD, HTN) and **TPS** (LAD, MR, Ischemia). Figure 13 shows the CE force-shortening for these three subjects with different heart diseases. The area encircled by the curve and the x-axis indicates the amount of energy generated by the CE.

In Figure 14, it is seen that the CE force-shortening velocity curve follows the same trend for all the subjects. The CE force and shortening-velocity both reach their maximal values at about one-third ejection. However, the loop made by HEL has the least area encircled within it, and correspondingly has the least contractile power input of the 3 subjects (as seen in Table 3).

5.2 Computation of the new contractility index, in comparison with the traditional contractility indices

Finally, we compute the traditional indices of contractility (EF and $dP/dt_{\max}$), and compare them with our proposed contractility index MSPI. Figures 15 and 16 show the correlation between MSPI and EF, and between MSPI and $dP/dt_{\max}$. The respective correlations are as followings: $MSPI = 55EF - 2.4$, (r=0.8905); dP/dt$_{max}MSPI = 0.04dP/dt_{\max} - 22$, (r=0.9054). These good correlations hence added credence to our newly formulated contractility index.

6 Concluding Remarks

In this study, LV systolic performance is investigated by means of a LV cylindrical-model mechatronic system of myocardial fiber located within the LV model wall The myocardial fibers are helically oriented within the LV model wall. Each myocardial fiber sarcomere unit is composed of three-elements: series element (analogue to connective tissue), viscous element (analogue to sarcolemma) and contractile element (analogue to sarcomere). The sarcomere contraction is associated with the relative sliding of the actin-myosin filaments.

The contractile force F_{CE} and shortening $x_2$of the LV myocardial-sarcomere unit are related to the LV pressure and volume data, and evaluated in terms of the model's parameters (k, B_v), and hence we can evaluate them. After that, we determine the in vivo characteristics of the LV sarcomere (CE), in terms of 'F_{CE} vs x_2' and 'F_{CE} vs $\dot{x}_2$', as well as the power generated by the sarcomere (CE). Both 'F_{CE} vs. $\dot{x}_2$' characteristics and the total contractile power input (TCPI) can be regarded as important LV functional indices.

Our evaluated in vivo CE force vs shortening and force vs shortening-velocity characteristics are seen to depict LV contractile function features: Less area encircled by the force-displacement and x-axis is associated with impaired LV contractility; Also, decreased area within the

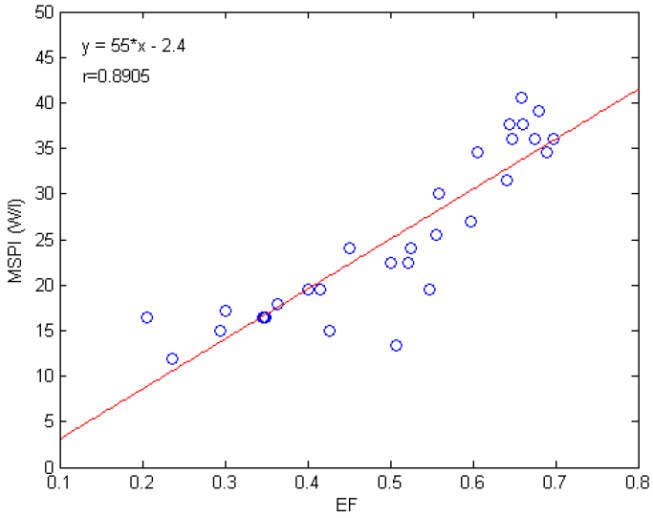

Figure 15 : Correlation of the myocardial sarcomeric power index (MSPI) to EF, the correlation coefficient r=0.8905.

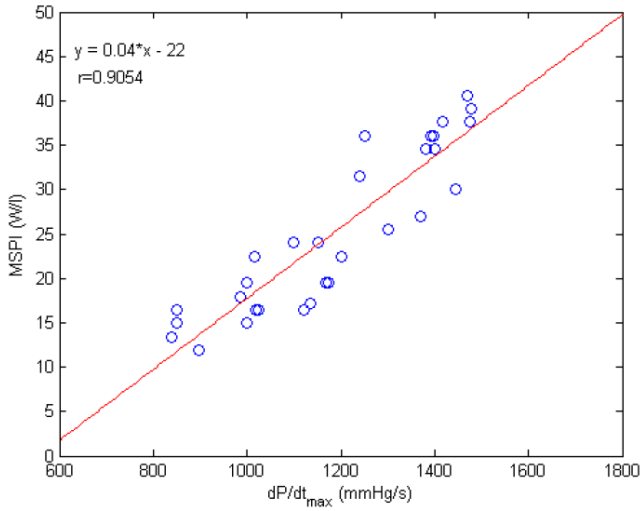

Figure 16 : Correlation of the myocardial sarcomeric power index (MSPI) to the traditional contractility index dP/dt_{max}, with the correlation coefficient r=0.9054.

force-shortening velocity curve is associated with less contractility; this indicates that a LV with impaired contractility is not able to generate as much power required to provide adequate EF and stroke volume as a properly-contracting LV.

Subject **HEL** has myocardial infarct, and hence has a weaker contracting myocardium. This is manifested by a lower CE maximal force and shortening-velocity, in comparison with subjects DDM and TPS (shown in Table 3). Correspondingly, its values of maximum power generated by CE, and the contractility index (MSPI) are lower than for the other two subjects. Also, the area of CE force-displacement curve for subject HEL is significantly less compared with the other two subjects. These results quantify how myocardial infarct impairs the left ventricular performance in terms of our model's contractile power-generated and contractility indices.

Subject **TPS** (with myocardial ischemia) has the maximal area encircled within its F_{CE} and $\dot{x}_2$ curve. This perhaps reflects an adaptive mechanism attempting to restore the LV performance, which is in agreement with its ejection fraction value (EF=0.68).

Table 3 summarizes all of these results. Figure 16 enables us to compare our MSPI index with the traditional contractility index $dP/dt_{\max}$. Even more significantly, our case studies for 30 subjects show that our new contractility index MSPI can be correlated with the traditional contraction index dP/dt_{max}, and hence can merit clinical employment.

Acknowledgement: We are grateful to Technician Mr. Ng Eng Hian from National Heart Centre, Singapore, for his technical assistance in cineangiographic recordings. This study was supported by grants from Strategic Development Scheme, Nanyang Technological University, Singapore.

References

Buckwalter, J. A.; Einhorn, T. A. and Simon, S. R. (2000): *Orthopaedic basic science: biology and biomechanics of the musculoskeletal system*, American Academy of Orthopaedic Surgeons.

Bulletti, C, (2001): *Human fertility and reproduction: the oocyte, the embryo, and the uterus*. New York, New York Acaemy of Science.

Ghista, D. N.; Advani, S. H.; Gaonkar, G. H.; Balachandran, K. and Brady, A. J. (1971): Analysis and physiological monitoring of human left ventricle. *J Basic Eng*, vol. 93, pp. 147-161.

Guyton, A. C. (1991): *Textbook of medical physiology*, Philadelp: Saunders.

Hoile, R. W. (1977): *Measurement and clinical importance of gastro-intestinal hormones*, Chelmsford U.K.

Ionescu, I.; Guilkey, J.; Berzins, M.; Kirby, R. M. and Weiss, J. (2005): Computational simulation of penetrat-

ing trauma in biological soft tissues using the material point method. *Stud Health Technol Inform*, vol. 111, pp. 213-218.

Hill, A. V. (1938): The heat of shortening and dynamic constants of muscle. *Pro R Soc London Ser B*, pp. 126-136.

Huxley, A. F. and Niedergerke, R. (1954): Structural changes in muscle during contraction. *Nature,*, vol. 173, pp. 971-973

Huxley, A. F. (1974): Muscular contraction: A review lecture. *J Physiol*, vol. 243, pp. 1-43.

Paladino, J. L. and Noordergraaf, A. (1998): Muscle contraction mechanism from ultrastructural dynamics. In: G. M. Drzewiecki; J. K. J. Li (ed) Analysis and assessment of cardiovascular function, Springer, Newyork, pp. 33-57.

Pietrabissa, R.; Montevecchi, F. M. and Funero, R. (1988): Ventricle mechanics based on sarcomere and fibre models. In: R. L. Spilker, B. R. Simon (ed) *Computational Methods in Bioengineering*, ASME, Newyork, BED 9, pp. 399-410.

Reconditi, M.; Linari, M.; Lucii, L.; Stewart, L. and Sun, Y. B. (2004): The myosin motor in muscle generates a smaller and slower working stroke at higher load. *Nature*, vol. 428, pp. 78-581.

Shoucri, R. M. (1990): The pressure-volume relation and mechanics of left ventricular contraction. *Jpn Heart J*, vol. 31, pp.713-729.

Shoucri, R. M. (1998): Studying the mechanics of left ventricle contraction. *IEEE Eng Biomed Eng*, vol. 17, pp. 95-101.

Shoucri, R. M. (2000): Active and passive stresses in the myocardium. *Am J Physiol Heart Circ Physiol*, vol. 279, pp. 2519-H2528.

Tan, A. M.; Zhong L.; Fuss, F. K. and Ghista, D. N. (2004): Biomechanics of push-up exercise and triceps contractility. *Proceedings of the 1st International Bioengineering Conference (IBEC)*, Singapore, pp. 308-311.

Xia, L.; Huo, M. M.; Wei, Q.; Liu, F. and Crozier, S. (2005): Analysis of cardiac ventricular wall motion based on a three-dimensional electromechanical biventricular model. *Phys Mod Biol*, vol. 50, pp. 1901-1917.

Zhong, L.; Ghista, D. N. and Ng, E. Y. K. (2004): Contractility of the left ventricle in terms of its sarcomere power generation. *Proceeding of the 1st International Bioengineering Conference (IBEC)*, Singapore, pp. 267-270.

Zhong, L.; Ghista, D. N.; Ng, E. Y. K. and Lim, S. K. (2005) Passive and active ventricular elastance of the left ventricle. *Biomedical Engineering Online*, pp. 4-10.

Zhong, L.; Ghista, D. N.; Ng, E. Y. K.; Lim, S. K. and Chua, T. S. J. (2004): Determination of aortic pressure-time profile, along with aortic stiffness and peripheral resistance. *J Mech Med Biol*, vol. 4, pp. 499-509.